



**HAL**  
open science

## Effect of antagonistic cable actuation on the stiffness of symmetric four-bar mechanisms

Vimalesh Muralidharan, Christine Chevallereau, Philippe Wenger, Nicolas J.S. Testard

► **To cite this version:**

Vimalesh Muralidharan, Christine Chevallereau, Philippe Wenger, Nicolas J.S. Testard. Effect of antagonistic cable actuation on the stiffness of symmetric four-bar mechanisms. CableCon 2023: Cable-Driven Parallel Robots, Jun 2023, Nantes, France. pp.332-343, 10.1007/978-3-031-32322-5\_27 . hal-04118861

**HAL Id: hal-04118861**

**<https://hal.science/hal-04118861v1>**

Submitted on 6 Jun 2023

**HAL** is a multi-disciplinary open access archive for the deposit and dissemination of scientific research documents, whether they are published or not. The documents may come from teaching and research institutions in France or abroad, or from public or private research centers.

L'archive ouverte pluridisciplinaire **HAL**, est destinée au dépôt et à la diffusion de documents scientifiques de niveau recherche, publiés ou non, émanant des établissements d'enseignement et de recherche français ou étrangers, des laboratoires publics ou privés.

# Effect of antagonistic cable actuation on the stiffness of symmetric four-bar mechanisms

Vimalesh Muralidharan, Christine Chevallereau, Philippe Wenger, and  
Nicolas J.S. Testard

Laboratoire des Sciences du Numérique de Nantes (LS2N), CNRS, 44321 Nantes,  
France

{Vimalesh.Muralidharan, Christine.Chevallereau, Philippe.Wenger,  
Nicolas.Testard}@ls2n.fr

**Abstract.** In biological systems, the joints are actuated antagonistically by muscles that can be moved coherently to achieve the desired displacement and co-activated with appropriate forces to increase the joint stiffness. Taking inspiration from this, there is an interest to develop bio-inspired robots that are suitable for both low-stiffness and high-stiffness tasks. Mechanisms actuated by antagonist cables can be a reasonable approximation of biological joints. A study on the anti-parallelogram mechanism showed that the antagonistic forces ( $> 0$ ) have a positive influence on its stiffness, similar to the biological joints. In this work, more general symmetric four-bar mechanisms with crossed/regular limbs, larger/smaller top and base bars are investigated for this property. Totally, six different types of mechanisms were identified and the limits of movement were determined in each case. Inside these limits, it was found through numerical simulations that the cable forces have a positive (resp. negative) influence on the stiffness of the mechanism when its limbs are crossed (resp. regular). This shows that the symmetric four-bar mechanisms with crossed limbs are suitable for building bio-inspired joints/robots, while their counterparts cannot serve this purpose. Among these, the anti-parallelogram mechanism offers the largest orientation range of  $]-\pi, \pi[$  for the top bar w.r.t. its base and is thus the best choice.

**Keywords:** four-bar mechanism · antagonistic actuation · cable-driven · stiffness

## 1 Introduction

There has always been an interest in developing robotic arms that are fast, accurate, repeatable, and energy efficient, for industrial applications. But, in the recent past, research on robotic arms with more sophisticated capabilities such as stiffness modulation, deployability, safe interaction with environment, have been gaining prominence [1],[2]. An important source of inspiration for developing such robots stems from the nature/biological systems, e.g., human arm in [3], giraffe's neck in [4], elephant's trunk in [5].

One of the key differences between the conventional robots and biological systems lies in their joints. While most of the robots are made up of revolute or prismatic joints, the biological systems hardly contain any of them. Instead, their joints are composed of complex surfaces in contact with one another. Some works have been dedicated exclusively to the study of kinematics such joints, e.g., human knee in [6], vertebrae of a bird’s neck in [7]. A review on the animal joints and their approximation with linkage mechanisms can be found in [8].

Another interesting feature of biological joints is their actuation. Unlike conventional robots with linear or rotary actuators, they are actuated antagonistically by muscles. Normally, one set of muscle(s) contract while their antagonistic counterparts relax and vice versa, to achieve the desired joint movement. But, under special circumstances, both sets of muscles contract simultaneously to increase the stiffness of the joint. This phenomenon is referred to as co-activation of muscles in biological systems [9].

This interesting actuation scheme has been adopted in variable stiffness actuators, where a pulley is used as the joint and two cables with in-series non-linear springs are used for antagonistic actuation [10]. The two cables are pulled simultaneously as in muscle co-activation, to enhance the stiffness of this joint. However, it must be emphasized that this is possible for the pulley joint only in the presence of non-linear springs [10].

There are other joints where stiffness modulation can be achieved without in-series springs, by only varying the cable forces, see e.g., the tensegrity-inspired joints presented in [11]. It was found that with the increase in antagonistic cable forces, the revolute joint experiences a drop in stiffness, which was a counter-intuitive result [11]. The same behavior was also reported for a 2R joint with offsets that represents one circle pure rolling over another [12]. In contrast, for an anti-parallelogram joint, that is equivalent to one ellipse pure rolling over another, the antagonistic actuation has a positive influence on the joint stiffness [11], just as in the biological joints. Thus, drawing inspiration from the anti-parallelogram mechanism, the goal of this work is to find all the four-bar mechanisms with symmetric limbs, that exhibit an increase in stiffness with antagonistic actuation by cables.

The remaining paper is organized as follows: the description of mechanism and cable arrangement is presented in Section 2. The kinematic and static models are discussed in Sections 3 and 4, respectively. The effect of antagonistic forces on the stiffness of various symmetric four-bar mechanisms are studied in Section 5. Finally, the conclusions are presented in Section 6.

## 2 Description of the symmetric four-bar mechanism

The schematics of four-bar mechanisms with symmetric limbs of length  $l$ , and a top bar of length  $b$  is shown in Fig. 1. The two pivots fixed to the ground are set at locations  $B_1(0, 0)$  and  $B_2(b_0, 0)$ , where  $b_0$  is a parameter that can be varied to produce different four-bar mechanisms. Notably,  $b_0 < 0$  produces mechanisms with crossed limbs, while  $b_0 > 0$  produces mechanisms with regular

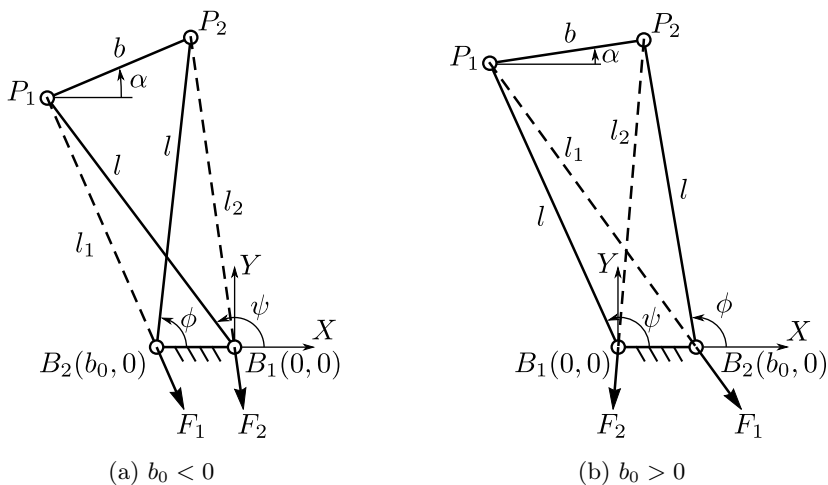


Fig. 1: Schematic diagram of four-bar mechanisms with symmetric limbs that are crossed when  $b_0 < 0$  (left) and regular when  $b_0 > 0$  (right). The two actuating cables are shown in dashed lines.

(non-crossed) limbs as illustrated in Figs. 1a and 1b, respectively. The special cases of anti-parallelogram and parallelogram mechanisms are obtained when  $b_0 = -b$  and  $b_0 = b$ , respectively. However, the case  $b_0 = 0$  degenerates the four-bar to a revolute joint and will not be considered in this work. For all the mechanisms, it is necessary that the geometric condition  $\left(l > \frac{|b-b_0|}{2}\right)$  be satisfied for its assembly.

This mechanism is actuated antagonistically with two cables  $C_1, C_2$ , connected between the pivots  $(P_1, B_2)$  and  $(P_2, B_1)$ , respectively, as indicated by dashed lines in Fig. 1. The force imparted by the cable  $C_i$  is given by  $F_i \geq 0$  and its varying length in the mechanism is denoted by  $l_i$ , for  $i = 1, 2$ . The cables are assumed to be massless and inelastic in this study.

The orientation of the top bar w.r.t. the base is denoted by  $\alpha$ , while those of the two limbs w.r.t. the base are given by  $\phi, \psi$ , respectively (see Fig. 1). The coordinate  $\alpha$  is used to measure the range of movement of the mechanism. The upper bound for  $\alpha$ , denoted by  $\alpha_{\max}$ , can be found by rotating the top bar from  $\alpha = 0$  in the counterclockwise direction until any of the three pivots  $(B_1, B_2, P_1, P_2)$  become collinear. Physically, at this configuration, the wrench imposed by one of the cables vanishes, and the static balance of the mechanism cannot be maintained. Thus, the wrench-feasible range of movement for this mechanism is given by  $\alpha \in ]-\alpha_{\max}, \alpha_{\max}[$ , owing to the symmetry in architecture and actuation scheme about  $\alpha = 0$ .

However, the above representation is not valid for the parallelogram mechanism ( $b_0 = b$ ), since  $\alpha$  remains zero at all the configurations. This case will be

treated separately in Section 5.1. But, for all other cases, further study will be conducted inside  $\alpha \in ] - \alpha_{\max}, \alpha_{\max}[$ .

### 3 Kinematic model of the mechanism

The loop-closure equation for the four-bar mechanism can be written as follows (see Fig. 1):

$$\overrightarrow{B_1P_1} + \overrightarrow{P_1P_2} - \overrightarrow{B_2P_2} - \overrightarrow{B_1B_2} = \vec{0} \quad (1)$$

This can be expanded into:

$$l \begin{pmatrix} \cos \psi \\ \sin \psi \end{pmatrix} + b \begin{pmatrix} \cos \alpha \\ \sin \alpha \end{pmatrix} - l \begin{pmatrix} \cos \phi \\ \sin \phi \end{pmatrix} - \begin{pmatrix} b_0 \\ 0 \end{pmatrix} = \begin{pmatrix} 0 \\ 0 \end{pmatrix} \quad (2)$$

Since the above equations are homogeneous in terms of the length parameter, it can be normalized by setting  $b = 1$ , without any loss of generality. Considering  $\alpha$  as the known input, it is possible to find the remaining angles  $(\phi, \psi)$  as a function of  $\alpha$  using the above equations (see e.g., [13], pp. 411-412). There are two possible solutions  $(\phi, \psi)_1$  and  $(\phi, \psi)_2$ , as presented below:

$$(\phi, \psi)_1 := \begin{cases} \cos \phi = \frac{\mu \sin \alpha + \cos \alpha - b_0}{2l} \\ \sin \phi = \frac{\sin \alpha + \mu(b_0 - \cos \alpha)}{2l} \\ \cos \psi = \frac{\mu \sin \alpha - \cos \alpha + b_0}{2l} \\ \sin \psi = \frac{\mu(b_0 - \cos \alpha) - \sin \alpha}{2l} \end{cases} \quad (\phi, \psi)_2 := \begin{cases} \cos \phi = -\frac{\mu \sin \alpha - \cos \alpha + b_0}{2l} \\ \sin \phi = -\frac{\mu(b_0 - \cos \alpha) - \sin \alpha}{2l} \\ \cos \psi = -\frac{\mu \sin \alpha + \cos \alpha - b_0}{2l} \\ \sin \psi = -\frac{\sin \alpha + \mu(b_0 - \cos \alpha)}{2l} \end{cases} \quad (3)$$

where  $\mu = \sqrt{\frac{4l^2 - b_0^2 - 1 + 2b_0 \cos \alpha}{b_0^2 + 1 - 2b_0 \cos \alpha}}$ . For a given  $\alpha \in ] - \alpha_{\max}, \alpha_{\max}[$ , one of the above solutions corresponds to the top bar  $P_1P_2$  being above the base  $B_1B_2$ , while the other corresponds to top bar being below the base. In this study, only the former solution is of interest. Note that the specified joint limits  $\alpha \in ] - \alpha_{\max}, \alpha_{\max}[$  preclude the case where one end of the top bar is above, while the other one is below.

By setting  $\alpha = 0$  in Eq. (3), it can be deduced from the resulting expressions that the desired solution branch is given by  $(\phi, \psi)_2$  when  $(b_0 < 1)$  and by  $(\phi, \psi)_1$  when  $(b_0 > 1)$ . Revoking the normalization w.r.t.  $b$ , the above conditions translate into  $(b_0 < b)$  and  $(b_0 > b)$  in the two cases, respectively.

From Fig. 1, the cable lengths (in all cases) can be written as follows:

$$\begin{cases} \text{Length of cable } C_1 \implies l_1 := P_1B_2 = \sqrt{l^2 + b_0^2 - 2lb_0 \cos \psi} \\ \text{Length of cable } C_2 \implies l_2 := P_2B_1 = \sqrt{l^2 + b_0^2 + 2lb_0 \cos \phi} \end{cases} \quad (4)$$

The lengths  $l_1, l_2$  can be obtained as functions of  $\alpha$  by substituting for  $\cos \psi$  and  $\cos \phi$  from Eq. (3), appropriately.

## 4 Static model of the mechanism

The static model of four-bar mechanism in Fig. 1 can be developed starting from its potential energy:

$$U = U_g + F_1 l_1 + F_2 l_2 \quad (5)$$

where  $U_g$  represents the contribution of gravity and springs (if any),  $F_i l_i$  with  $i = 1, 2$  represents the work potential of the actuating cables. Treating  $\alpha$  as the generalized coordinate in this study, differentiating  $U$  w.r.t.  $\alpha$  and setting it to 0, yields the static equilibrium equation:

$$\frac{dU_g}{d\alpha} + F_1 \frac{dl_1}{d\alpha} + F_2 \frac{dl_2}{d\alpha} = 0 \quad (6)$$

Further differentiation w.r.t.  $\alpha$  yields the stiffness ( $K$ ) of the mechanism:

$$K := \frac{d^2 U_g}{d\alpha^2} + F_1 \frac{d^2 l_1}{d\alpha^2} + F_2 \frac{d^2 l_2}{d\alpha^2} \quad (7)$$

Since the stiffness must be evaluated only when the equilibrium equation is satisfied, one can solve for  $F_2$  from Eq. (6) and substitute into Eq. (7), to obtain:

$$K = \gamma_1 F_1 + \text{other terms} \quad (8)$$

where  $\gamma_1 = \left( \frac{d^2 l_1}{d\alpha^2} + \left( \frac{-dl_1/d\alpha}{dl_2/d\alpha} \right) \frac{d^2 l_2}{d\alpha^2} \right)$ . Similarly, it is also possible to solve for  $F_2$  from Eq. (6) and substitute in Eq. (7) to obtain the coefficient of  $F_2$  in  $K$  as  $\gamma_2 = \left( \frac{d^2 l_2}{d\alpha^2} + \left( \frac{-dl_2/d\alpha}{dl_1/d\alpha} \right) \frac{d^2 l_1}{d\alpha^2} \right)$ .

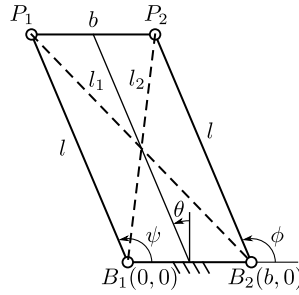
The effect of actuation forces on stiffness can be studied based on the terms  $\gamma_1$  and  $\gamma_2$ . If  $\gamma_1 > 0$  (resp.  $\gamma_2 > 0$ ), it implies that  $F_1$  (resp.  $F_2$ ) has a positive influence on the stiffness. Similarly, if they are negative then forces have a negative influence on the stiffness. Due to symmetry in the architecture and cable connections,  $\gamma_1$  and  $\gamma_2$  are mutually symmetric about  $\alpha = 0$ .

Mechanisms with positive  $\gamma_1, \gamma_2$ , are quite interesting because even when they become unstable due to external factors such as an increase in payload, they can be stabilized by simply increasing the actuation forces. This key property makes them ideal candidates for mimicking muscle actuated joints in biological systems, e.g., elbow joint of a human arm, where its increased stability can be felt by simultaneous contraction of the associated muscles.

In the subsequent sections, the nature of  $\gamma_1, \gamma_2$  is studied for various four-bar mechanisms.

## 5 Effect of actuation forces on stiffness

The effects of antagonistic forces on the stiffness of parallelogram and anti-parallelogram mechanisms are studied in Section 5.1, while the effects on general symmetric four-bar mechanisms are studied in Section 5.2.

Fig. 2: Schematic of the parallelogram mechanism ( $b_0 = b$ ).

### 5.1 Parallelogram and anti-parallelogram mechanisms

The parallelogram mechanism shown in Fig. 2 is obtained by setting  $b_0 = b$ . Unlike other four-bar mechanisms,  $\alpha$  remains 0 at all configurations for this mechanism. Hence, the orientation ( $\theta$ ) of the line joining mid points of the top and base bars w.r.t. the vertical, is used as the independent coordinate. The range of movement is limited by  $\theta \in ]-\frac{\pi}{2}, \frac{\pi}{2}[$ , due to the flat-singularities.

From Fig. 2, it is apparent that  $\phi = \psi = \frac{\pi}{2} + \theta$ . Thus, from Eq. (4), the cable lengths are given by:

$$l_1 = \sqrt{l^2 + b^2 + 2lb \sin \theta} \quad l_2 = \sqrt{l^2 + b^2 - 2lb \sin \theta} \quad (9)$$

Following the same process described in Section 4, with  $\theta$  in place of  $\alpha$ , one obtains  $\gamma_1, \gamma_2$  as:

$$\begin{cases} \gamma_1 = -\frac{2b\lambda^2(\lambda^2+1)\cos^2(\theta)}{(\lambda^2+1-2\lambda\sin\theta)(\lambda^2+1+2\lambda\sin\theta)^{3/2}} \\ \gamma_2 = -\frac{2b\lambda^2(\lambda^2+1)\cos^2(\theta)}{(\lambda^2+1-2\lambda\sin\theta)^{3/2}(\lambda^2+1+2\lambda\sin\theta)} \end{cases} \quad (10)$$

where  $\lambda = (l/b)$ . It is apparent that all the factors in the numerators of  $\gamma_1$  and  $\gamma_2$  are positive. The two factors in the denominators are also positive since they are bounded inside  $[(\lambda-1)^2, (\lambda+1)^2]$  for all real  $\theta$ . Thus, it is clear that  $\gamma_1, \gamma_2 < 0$ , due to the leading negative sign. This shows that antagonistic forces have a negative impact on the stiffness of the parallelogram mechanism. This result is consistent with the experimental data presented in [14], which shows that the cable tensions were reduced to increase the stiffness of this mechanism.

Contrary to the parallelogram mechanism, it has been proven analytically in [11] that the antagonistic forces have a positive impact on the stiffness of anti-parallelogram mechanism.

As a numerical illustration consider a parallelogram ( $b_0 = b$ ) and an anti-parallelogram ( $b_0 = -b$ ) mechanism with  $b = 1$  m and  $l = 2$  m each. For the sake of simplicity, the bar masses are neglected and no springs are added to these mechanisms. In order to perform a fair comparison, the anti-parallelogram mechanism will also be described by the coordinate  $\theta$ , as defined above for the parallel-

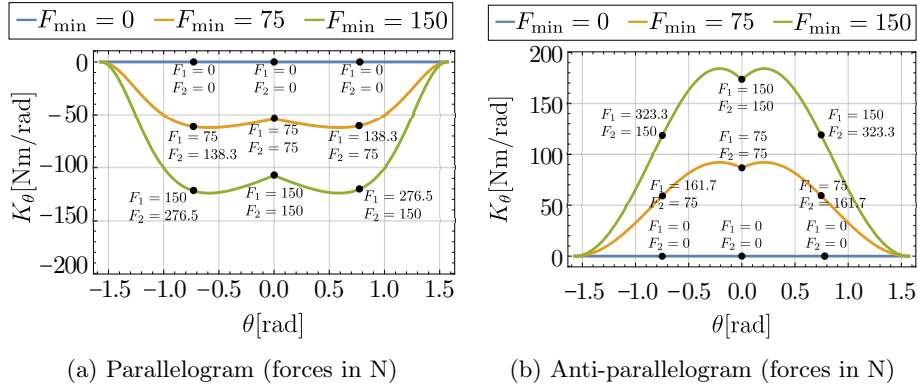


Fig. 3: Stiffness of the mechanisms when  $\theta \in ]-\frac{\pi}{2}, \frac{\pi}{2}[$  for different actuation forces.

ogram mechanism. The associated expressions for cable lengths and mechanism stiffness can be found in [11].

One of the ways to study the change in stiffness with increasing antagonistic forces is to firstly specify a minimum value for the actuation forces, say  $F_{\min}$ . At a given configuration  $\theta$ , one could compute the balancing forces  $(F_1, F_2)$  from Eq. (6) (neglecting  $U_g$ ) such that one of them is equal to  $F_{\min}$  while the other is greater than or equal to  $F_{\min}$ . These forces can be substituted in Eq. (7) to find the respective value of stiffness. This process has been carried for different values of  $F_{\min}$ : 0 N, 75 N and 150 N. The corresponding values of stiffness are plotted for the parallelogram and anti-parallelogram mechanisms in Fig. 3a and 3b, respectively. The equilibrium forces are also represented at certain configurations. It is apparent that an increase in  $F_{\min}$  causes a decrease (resp. increase) in stiffness for the parallelogram (resp. anti-parallelogram) mechanism, for all values of  $\theta$ . This is a consequence of the negative (resp. positive) force coefficients  $\gamma_1, \gamma_2$  for the parallelogram (resp. anti-parallelogram) mechanism. This shows that the anti-parallelogram mechanism can serve as a bio-inspired joint while the parallelogram mechanism cannot.

## 5.2 General symmetric four-bar mechanisms

Unlike the parallelogram and anti-parallelogram mechanisms, it is very difficult to conduct analytical studies on  $\gamma_1, \gamma_2$  for the general mechanisms ( $b_0 \neq \pm b$ ) due to the emergence of nested square roots in expressions of  $l_1, l_2$  (see Eqs. (3),(4)). Hence, the nature of  $\gamma_1, \gamma_2$  will be studied through numerical examples for these mechanisms. Firstly, six different cases I, ..., VI have been identified based on the value of  $b_0$ , as shown in Tables 1 and 2. In each case, the limiting configurations at  $(\pm\alpha_{\max})$ , plot of  $\gamma_1, \gamma_2$  inside  $\alpha \in ]-\alpha_{\max}, \alpha_{\max}[$  for one candidate design, and the limiting value of  $\gamma_1, \gamma_2$  inside the feasible design space, are presented



in the successive columns of these tables. The following observations are made from them:

- The maximum orientation of top bar  $\alpha_{\max}$  varies in  $]0, \pi[$  for the mechanisms in cases (I, II, III), while it is limited to  $[0, \frac{\pi}{2}[$  in cases (IV, V, VI). Thus, mechanisms with crossed limbs must be preferred for applications requiring large  $\alpha$ .
- From the plots of  $\gamma_1, \gamma_2$  for one candidate design, it is observed that they remain non-negative (resp. non-positive) for cases (I, II, III) (resp. (IV, V, VI)). The values of  $\gamma_1, \gamma_2$  tend to  $\pm\infty$  near the boundary, in cases (I, III, IV, VI) due to the vanishing of  $\frac{dl_1}{d\alpha}$  or  $\frac{dl_2}{d\alpha}$ , present in the denominator of the respective expressions (see below Eq. (8)). However,  $\gamma_1, \gamma_2$  remain bounded and tend to 0 in cases (II, V) due to the vanishing of both first derivatives of  $l_1, l_2$  at the boundary.
- In order to verify if  $\gamma_1, \gamma_2$  remain positive (resp. negative) for other designs in cases (I, II, III) (resp. (IV, V, VI)), their minimum  $\gamma_{\min}$  (resp. maximum  $\gamma_{\max}$ ) inside the range of movement is tested. Since the expressions of  $\gamma_1, \gamma_2$  are homogeneous w.r.t. the derivatives of cable lengths, one of the length variables ( $b \neq 0$ ) can be factored out as in Eq. (10). This reduces the design space to just two variables  $(\frac{l}{b}, \frac{b_0}{b})$ . Firstly, a feasible design space satisfying the assembly condition  $l > \frac{|b-b_0|}{2}$  and bounded by  $0 < \frac{l}{b}, \frac{|b_0|}{b} \leq 20$  is constructed. The values of  $\frac{\gamma_{\min}}{b}$  and  $\frac{\gamma_{\max}}{b}$  are computed for the feasible designs numerically to obtain the plots in last columns of the two tables. From these, it is clear, that  $\gamma_{\min} \geq 0$  for cases (I, II, III) and  $\gamma_{\max} \leq 0$  for cases (IV, V, VI). This illustrates that the antagonistic forces have a positive (resp. negative) influence on the stiffness of mechanisms with crossed (resp. regular) limbs.
- Among the four-bar mechanisms with a positive correlation between forces and stiffness, the anti-parallelogram (case II) has the largest range of movement  $\alpha \in ]-\pi, \pi[$  and is to be preferred in general. However, the mechanisms in cases (I, III) might also be interesting for applications where large orientation range may not be essential, e.g., joints in the hyper redundant robots inspired from elephant's trunk [5]. In cases (I, III) the value of  $\gamma_{\min}$  is large for designs close to the limiting assembly condition  $2l = |b - b_0|$ , which indicates that there is a compromise between the range of movement and  $\gamma_{\min}$  in these designs.

## 6 Conclusion

A class of four-bar mechanisms with symmetric limbs, actuated antagonistically with two cables imposing forces  $F_1, F_2 > 0$ , has been considered in this work. The effect of an actuation force  $F_1$  (resp.  $F_2$ ) on the stiffness a mechanism has been studied through its coefficient  $\gamma_1$  (resp.  $\gamma_2$ ) in the expression of stiffness after eliminating the other force  $F_2$  (resp.  $F_1$ ) using the equilibrium equation. Due to the symmetry in architecture and arrangement of cables, the force coefficients

Table 1: Effect of antagonistic forces on the stiffness of four-bar mechanisms with ( $b_0 < 0$ ) (crossed limbs).

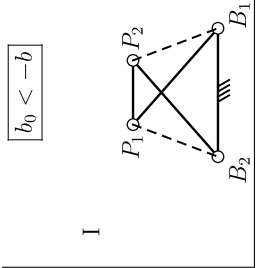
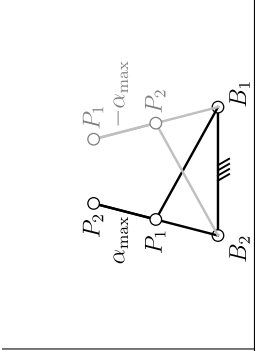
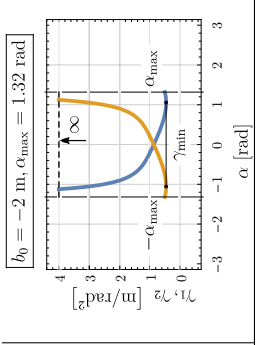
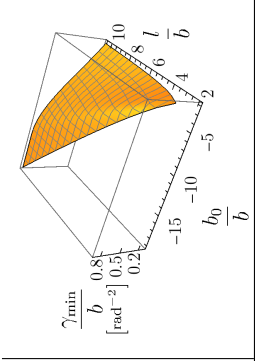
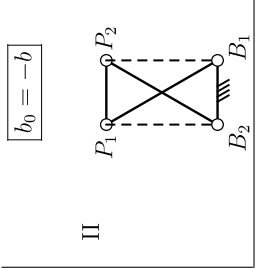
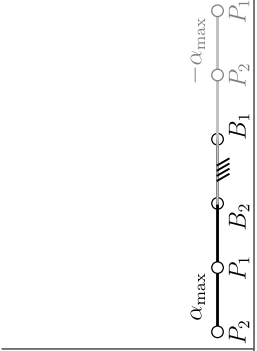
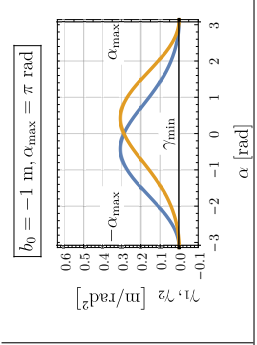
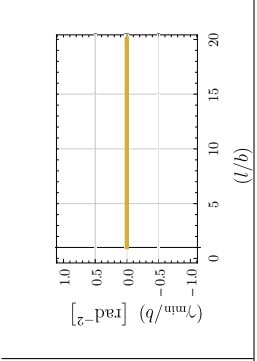
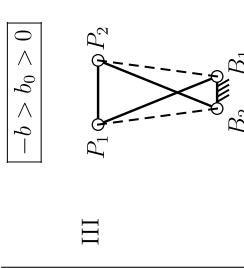
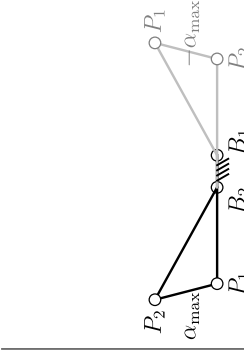
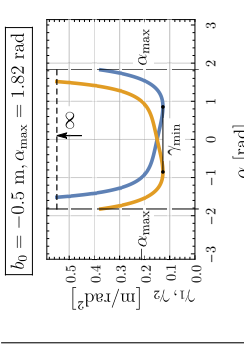
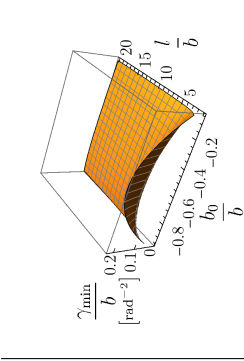
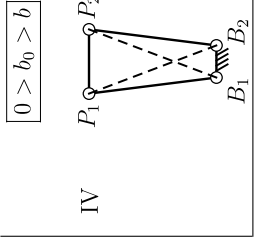
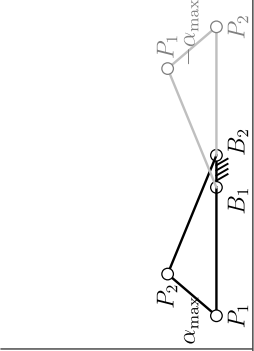
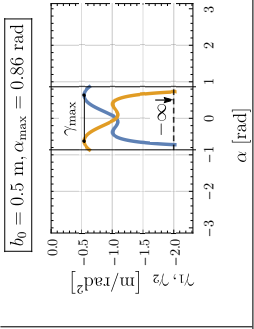
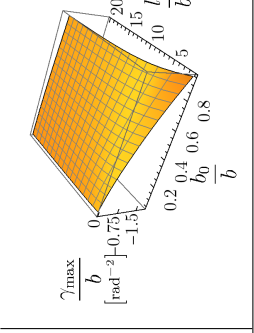
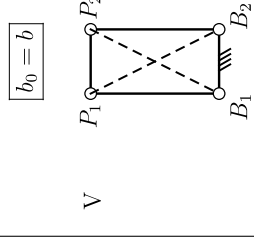
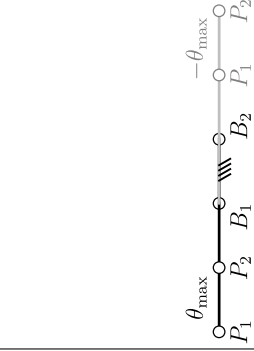
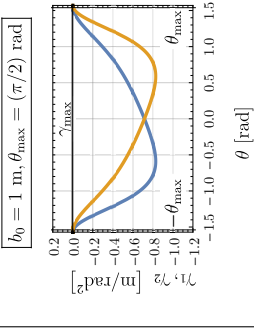
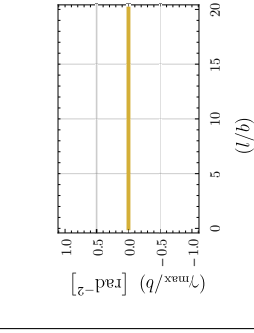
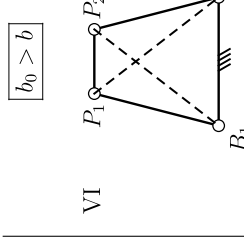
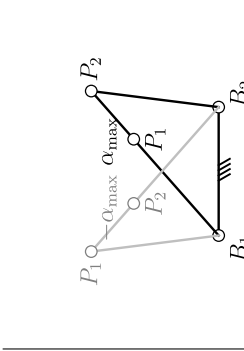
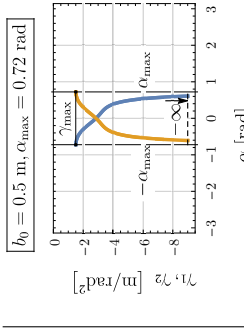
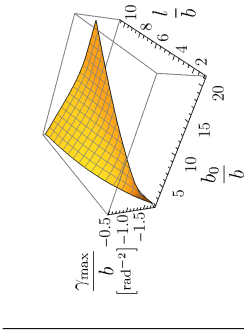
Condition/ Schematic	Bounds on $\alpha \in [-\alpha_{\max}, \alpha_{\max}]$	Plot of $\gamma_1, \gamma_2$ for one design with $b = 1$ m, $l = 2$ m	$(\gamma_{\min}/b)$ in design space $2l >  b - b_0 $ & $l,  b_0  \in [0, 20]b$
<p>I</p>  <p><math>b_0 &lt; -b</math></p>	 <p><math>\alpha_{\max}</math> <math>-\alpha_{\max}</math></p>	 <p><math>b_0 = -2</math> m, <math>\alpha_{\max} = 1.32</math> rad</p>	
<p>II</p>  <p><math>b_0 = -b</math></p>	 <p><math>\alpha_{\max}</math> <math>-\alpha_{\max}</math></p>	 <p><math>b_0 = -1</math> m, <math>\alpha_{\max} = \pi</math> rad</p>	
<p>III</p>  <p><math>-b &gt; b_0 &gt; 0</math></p>	 <p><math>\alpha_{\max}</math> <math>-\alpha_{\max}</math></p>	 <p><math>b_0 = -0.5</math> m, <math>\alpha_{\max} = 1.82</math> rad</p>	

Table 2: Effect of antagonistic forces on the stiffness of four-bar mechanisms with ( $b_0 > 0$ ) (regular limbs).

Condition/ Schematic	Bounds on $\alpha \in [-\alpha_{\max}, \alpha_{\max}]$	Plot of $\gamma_1$ , $\gamma_2$ for one design with $b = 1$ m, $l = 2$ m	$(\gamma_{\min}/b)$ in design space $2l >  b - b_0 $ & $l,  b_0  \in [0, 20b]$
IV 			
V 			
VI 			

are also mutually symmetric about the configuration where the top and base bars are parallel. When  $\gamma_1, \gamma_2$  are positive, the stiffness increases with the increase in cable forces, similar to the muscle actuation of a biological joint.

It was found through numerical simulations that  $\gamma_1, \gamma_2 > 0$  occurs only when the two limbs are crossed, and not otherwise. Among such mechanisms, the anti-parallelogram mechanism offers the largest orientation range of  $]-\pi, \pi[$  for the top bar w.r.t. its base, and is thus best suited for building bio-inspired robot manipulators. The other mechanisms with crossed limbs might also be of interest for applications where large range of movement is not a necessity, as in redundant and hyper-redundant systems.

The formulation of stiffness showed that the effect of actuation forces depends only on the varying cable lengths in the mechanism and its first, second order derivatives. Hence, it would be interesting to search for more general conditions on the instantaneous properties of actuation force lines and the instant center of rotation, to have a positive correlation between actuation and stiffness. For the four-bar mechanisms, it is well known that the movement of its coupler w.r.t. the base can be represented by the pure rolling of one curve (moving centrode) over another (fixed centrode) [15]. A study of the nature of these curves and the cable force lines in each case might provide a more intuitive understanding of the co-activation phenomenon, and aid in the development of more such mechanisms (with one or more degrees of freedom) for bio-inspired robots.

## References

1. Boucher, G., Laliberté, T., Gosselin, C.: Mechanical design of a low-impedance 6-degree-of-freedom displacement sensor for intuitive physical human–robot interaction. *Journal of Mechanisms and Robotics* **13**(2) (2021).
2. Palmieri, P., Melchiorre, M., Mauro, S.: Design of a lightweight and deployable soft robotic arm. *Robotics* **11**(5), 88 (2022).
3. Liu, F., Xu, W., Huang, H., Ning, Y., Li, B.: Design and analysis of a high-payload manipulator based on a cable-driven serial-parallel mechanism. *Journal of Mechanisms and Robotics* **11**(5) (2019).
4. Niikura, A., Nabae, H., Endo, G., Gunji, M., Mori, K., Niiyama, R., Suzumori, K.: Giraffe neck robot: First step toward a powerful and flexible robot prototyping based on giraffe anatomy. *IEEE Robotics and Automation Letters* **7**(2), 3539–3546 (2022).
5. Liu, Y., Ge, Z., Yang, S., Walker, I.D., Ju, Z.: Elephant’s trunk robot: An extremely versatile under-actuated continuum robot driven by a single motor. *Journal of Mechanisms and Robotics* **11**(5) (2019).
6. Parenti-Castelli, V., Sancisi, N.: Synthesis of spatial mechanisms to model human joints. In: McCarthy, J.M. (ed.) *21st Century Kinematics*. pp. 49–84. Springer London, London (2013)
7. Furet, M., Abourachid, A., Böhmer, C., Chummun, V., Chevallereau, C., Cornette, R., De La Bernardie, X., Wenger, P.: Estimating motion between avian vertebrae by contact modeling of joint surfaces. *Computer Methods in Biomechanics and Biomedical Engineering* **25**(2), 123–131 (2022).
8. Burgess, S.: A review of linkage mechanisms in animal joints and related bioinspired designs. *Bioinspiration & Biomimetics* **16**(4), 041001 (2021).

9. Latash, M.L.: Muscle coactivation: definitions, mechanisms, and functions. *Journal of Neurophysiology* **120**(1), 88–104 (2018).
10. Vanderborght, B., Albu-Schaeffer, A., Bicchi, A., Burdet, E., Caldwell, D., Carloni, R., Catalano, M., Eiberger, O., Friedl, W., Ganesh, G., Garabini, M., Grebenstein, M., Grioli, G., Haddadin, S., Hoppner, H., Jafari, A., Laffranchi, M., Lefeber, D., Petit, F., Stramigioli, S., Tsagarakis, N., Van Damme, M., Van Ham, R., Visser, L., Wolf, S.: Variable impedance actuators: A review. *Robotics and Autonomous Systems* **61**(12), 1601–1614 (2013).
11. Muralidharan, V., Wenger, P.: Optimal design and comparative study of two antagonistically actuated tensegrity joints. *Mechanism and Machine Theory* **159**, 104249 (2021).
12. Muralidharan, V., Testard, N. J. S., Chevallereau, C., Abourachid, A., Wenger, P.: Variable stiffness and antagonist actuation for cable-driven manipulators inspired by the bird neck. *Journal of Mechanisms and Robotics* (in review)
13. McCarthy, J.M., Soh, G.S.: *Geometric Design of Linkages*. Springer-Verlag, New York, 2 edn. (2010)
14. Boehler, Q., Abdelaziz, S., Vedrines, M., Poignet, P., Renaud, P.: Towards the control of tensegrity mechanisms for variable stiffness applications: A case study. In: Wenger, P., Flores, P. (eds.) *New Trends in Mechanism and Machine Science*. pp. 163–171. Springer International Publishing, Cham (2017)
15. Norton, R. L.: *Design of machinery: an introduction to the synthesis and analysis of mechanisms and machines*. McGraw-Hill, New York, 6 edn. (2019)